

# Compact Precision Laser Inclinometer: Measurement of Signals and Noise

N. V. Atanov<sup>a</sup>, I. V. Bednyakov<sup>a</sup>, Yu. A. Budagov<sup>a</sup>, V. V. Glagolev<sup>a</sup>, Yu. V. Klemeshov<sup>a</sup>,  
A. V. Krasnoperov<sup>a</sup>, A. M. Kuzkin<sup>a</sup>, M. V. Lyablin<sup>a</sup>\*, R. V. Ni<sup>a</sup>, A. A. Pluzhnikov<sup>a</sup>, K. D. Polyakov<sup>a</sup>,  
A. A. Seletsky<sup>b</sup>, G. V. Trubnikov<sup>a</sup>, and B. Di Girolamo<sup>b</sup>

<sup>a</sup> Joint Institute for Nuclear Research, Dubna, Russia

<sup>b</sup> European Organization for Nuclear Research (CERN), Geneva, Switzerland

\*e-mail: lyablin@jinr.ru

Received January 18, 2023; revised February 15, 2023; accepted February 15, 2023

**Abstract**—The results of developing a compact version of the Precision Laser Inclinometer (CPLI) with the reduced overall dimensions of  $20 \times 20 \times 20$  cm and weight of 10 kg are presented. Experimental data on detected angular oscillations of the Earth's surface at the JINR site are obtained. The achieved sensitivity is  $6 \times 10^{-11}$  rad/Hz<sup>1/2</sup> in the frequency range  $1.4 \times 10^{-3}$ –10 Hz. The CPLI can be used in modern physical experiments for seismic isolation of large-scale installations. Reduction of the impact of microseismic angular oscillations of the Earth's surface on the sensitive elements of the VIRGO Interference Gravitational Antenna, the Large Hadron Collider, and NICA will increase the accuracy of the experiments.

DOI: 10.1134/S1063779623040068

## INTRODUCTION

To improve the measurement accuracy in a modern large-scale physical experiment, it is required to reduce the influence of the angular inclinations of the earth's surface caused by surface seismic waves [1–4]. This phenomenon leads to a shift in the foci of particle beams in colliders and to noise oscillations of suspended mirrors in interferometric gravitational antennas.

To solve these problems, a new precision method for measuring changes in the tilt angles of the Earth's surface was invented at JINR – the Precision Laser Inclinometer (PLI) [5]. The achieved measurement accuracy of the PLI is  $2.4 \times 10^{-11}$  rad/Hz<sup>1/2</sup> in the frequency range  $10^{-3}$ –10 Hz [6–10].

The first generations of PLI had large dimensions of  $50 \times 40 \times 30$  cm and a weight of more than 60 kg. It was also necessary to take into account the amount of electronics for its maintenance. Often, it is difficult to find a place for the PLI with the indicated dimensions and weight in a physical experiment. Therefore, it became necessary to significantly reduce the overall dimensions and the weight of the inclinometer.

To create a compact PLI (CPLI), it was necessary to change the optical scheme of the PLI, use temperature-resistive elements in the design of the CPLI, etc. [11, 12].

The article discusses the main characteristics of a new type of inclinometer—the CPLI.

## METHODOLOGY OF THE PRECISION LASER INCLINOMETER

The PLI is based on the property of the liquid surface to be leveled when the earth's surface is tilted. In this case, the surface of the horizontalized liquid is perpendicular to the Earth's gravity vector.

The gravity vector experiences angular inclinations due to external forces caused by the Moon, the Sun, and surrounding massive objects (mountains, reservoirs). For registration of changes in the slope of the earth's surface, they are of minor importance due to the extremely low frequencies of their impact. In registration of changes in the slopes of the earth's surface in the frequency range of  $10^{-3}$ –20 Hz, these phenomena are conditionally constant and do not change the magnitude of the slopes of the earth's surface. The influence of the Moon and the Sun occurs with a period of  $\approx 12$  h and covers an area with a diameter of more than 5000 km (Fig. 1) [13, 14]. The use of the PLI in a relatively small area of  $10 \times 10$  km causes the identical slope for all inclinometers. This makes it possible to take into account inclinations of the earth's surface due to the Moon and the Sun in the readings of all inclinometers operating in this area.

The second feature of the PLI is the use of a thin layer  $d$  of a liquid in the inclinometer cuvette (Fig. 2) [5, 15, 16]. Under the condition  $d \ll \lambda_w$ , where  $\lambda_w$  is the length of the surface wave, propagation of surface waves is suppressed due to their large friction on the

bottom of the cuvette. Experience shows that this condition works in the entire PLI frequency range.

Horizontalization of the inclinometer occurs due to the effect of the communicating vessels [17, 18]. With a sharp inclination of the cuvette, an inertial change in the position of the liquid surface occurs, which subsequently returns it to a horizontal position. In this case, the liquid in the cuvette moves in the vertical direction. This feature makes horizontalization a fairly fast process (Fig. 3).

From the formula for the natural frequency  $\nu$  of oscillations in communicating vessels

$$\nu = \frac{1}{2\pi} \sqrt{\frac{g}{d}} \tag{1}$$

where  $g$  is the acceleration of free fall,  $d$  is the thickness of the liquid layer, we determine the limiting frequency  $\nu$  of the liquid surface oscillations. For a liquid layer with  $d = 1$  mm, the frequency  $\nu$  is 16 Hz.

The horizontalization time is half the period of fluid oscillations in communicating vessels

$$T_{\text{hor}} = \frac{1}{2\nu} \tag{2}$$

and equal to  $T_{\text{hor}} = 0.03$  s. Actually,  $T_{\text{hor}}$  defines “dead time”, during which the surface of the liquid is unstable.

This indicates a potentially high maximum recorded frequency ( $\approx 20$  Hz) of the Earth’s surface oscillations in the PLI.

Thus, we have a stable reference surface perpendicular to the gravity vector, relative to which we can measure the slopes of the earth’s surface.

The physical limitation for PLI sensitivity is the statistical change in the volume of the liquid, which locally changes the slopes of the liquid surface. The estimates obtained in [19] make it possible to limit the sensitivity of the inclinometer for water to  $4 \times 10^{-11}$  rad.

### REGISTRATION OF SLOPES OF THE EARTH’S SURFACE BY THE PLI METHOD

To register the slopes of the earth’s surface, we use the reflection of a laser beam from the liquid surface (Fig. 4).

A laser, a cell with liquid and a Position Sensitive Photodetector (PSD) are fixed on the surface of the Earth. When the earth’s surface is tilted by an angle  $\gamma$ , the reflected laser beam is displaced relative to the PSD by a double angle  $2\gamma$  (Fig. 4). This allows one to simultaneously measure the angular changes in the tilt of the Earth’s surface in two orthogonal directions. Such angular changes are fixed with a certain time interval and are signals in the Precision Laser Inclinometer.

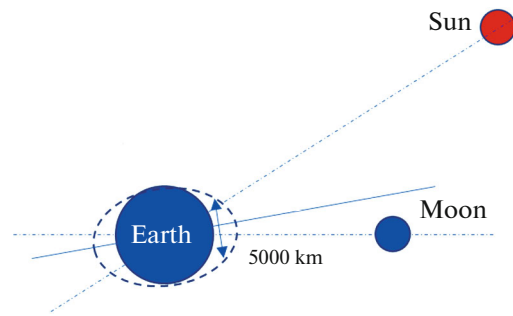


Fig. 1. Change in the angular inclinations of the Earth’s surface by the Moon and the Sun.

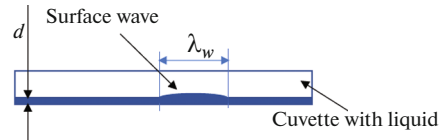


Fig. 2. Suppression of surface waves in a thin liquid layer.

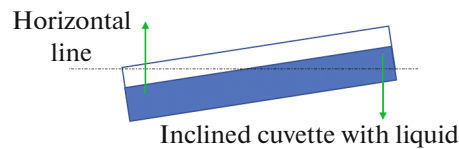


Fig. 3. Liquid leveling.

The recorded PLI signals determine the angular evolution of the inclinations of the earth’s surface in time. It is this feature of the PLI that makes it possible to use it to reduce the influence of the angular inclinations of the earth’s surface in a physical experiment and also to determine the temporal evolution of changes in the landscape of the earth’s surface.

## THE HISTORY OF THE CREATION OF THE PLI

### First-Generation PLI

At the first stage (2010), the physical conditions were determined under which the liquid surface in the

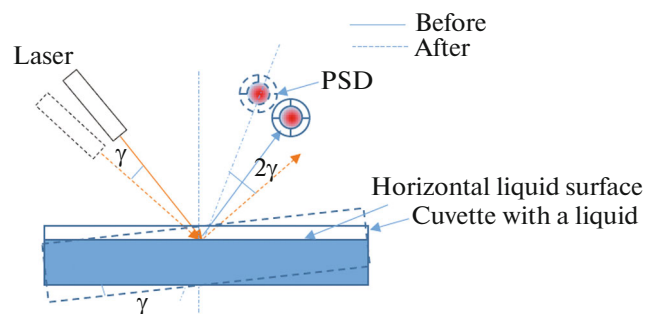


Fig. 4. Registration of the slopes of the earth’s surface by the PLI method.

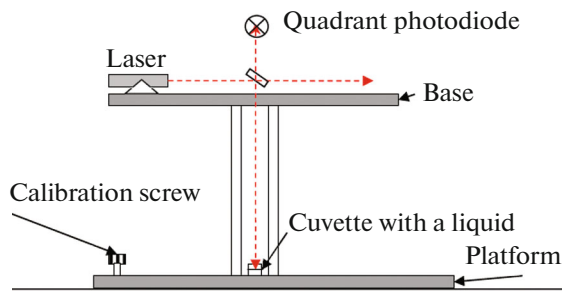


Fig. 5. Scheme of the first-generation PLI.

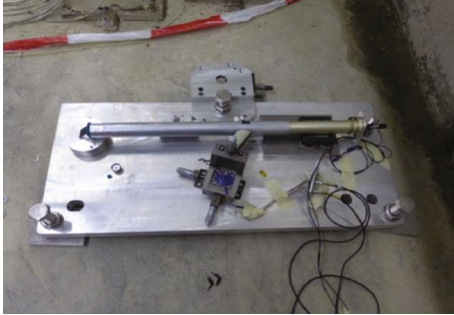


Fig. 6. PLI of the second generation.

PLI cell remains stable. The first microseismic signals of distant earthquakes were detected at the installation (Fig. 5) [20]. In 2012 a patent for inventions was obtained [5], which fixed the idea of using a thin layer of liquid to stabilize the surface of the liquid when registering the slopes of the earth's surface.

### Second-Generation PLI

The second important step was the use of the effect of reducing fluctuations in the laser beam cross section caused by turbulent changes in the air medium. Previously, we discovered the effect of stabilizing the

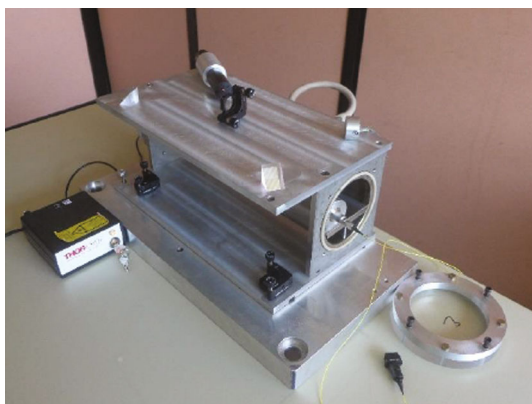


Fig. 7. PLI of the third generation.

direction of a laser beam as it propagates in a pipe [21]. A patent [22] was obtained, which fixed the priority in using this effect. The first inclinometer was built (Fig. 6), on which for the first time angular oscillations of the Earth's surface were effectively detected online during the passage of surface microseismic waves of the "Microseismic Peak" type.

### Third-Generation PLI

The next important step was the use of vacuum (2015) to stabilize the position of the laser beam. The vacuum made it possible to remove dust from the air and significantly reduced the effect of fluctuations in the refractive index of the air on the accuracy of PLI measurements. Vacuuming the PLI sensing element significantly improved the sensitivity of the device. Also, registration of the angular wandering of the laser beam by a separate channel was introduced (Fig. 7). Convincing evidence has been obtained for the registration of the inclinations of the earth's surface by the Moon and the Sun for three days (Fig. 8) [23].

In Fig. 8, the angular oscillations of the Earth's surface due to the Moon and the Sun recorded with the PLI (Fig. 7) in two orthogonal planes are compared with the measurements made using the Hydrostatic Level System (HLS) 150 m long [24]. One of the PLI detection directions coincided with that of the HLS. For the first time, angular inclinations of the Earth's surface due to the Moon and the Sun were simultaneously recorded in two orthogonal planes by a compact inclinometer.

### Fourth- and Fifth-Generation PLI

In the next two generations of the PLI (Figs. 9, 10), methods for remote control of the inclinometer and signal recording were developed. This made it possible to remotely monitor the microseismic activity of the Earth and to start implementing a network of simultaneously recording PLIs.

For the period 2010–2020, the evolution of the PLI included 5 generations. The last two PLI generations operate at the Garni International Geophysical Center (Armenia) (1 PLI), at CERN (5 PLIs) and on the VIRGO Gravity Antenna (2 PLIs).

### Sixth-Generation PLI

The sixth generation of PLI is a Compact Precision Laser Inclinometer (CPLI).

Figure 11 shows the appearance of the sensitive element of the CPLI.

We hope that CPLI will significantly change both the possibilities of using the device and the accuracy of the data obtained.

COMPACT PRECISION LASER INCLINOMETER

Previous generations of the Precision Laser Incliner had dimensions that did not allow it to be used in the conditions of the VIRGO Interferometric Gravity Antenna and the LHC tunnel, which restricted its further applications. It was required to sharply reduce the dimensions and weight of the inclinometer.

To place the PLI on the sensitive elements of the gravitational antenna and inside the LHC tunnel, its dimensions must be less than  $20 \times 20 \times 20$  cm and weight of about 10 kg.

*Ways to Ensure the Compact Size of the PLI*

The main problem of reducing the dimensions of the PLI is associated with the use of a quadrant photodetector to detect the displacement of the laser beam. The PLI uses a focused laser beam with a focal spot diameter of less than  $100 \mu\text{m}$ . A square photodetector has a dielectric gap between photodetectors, which has a minimum size of  $30 \mu\text{m}$  [25]. This is what does not allow reducing the diameter of the laser beam to less than 100 microns and, accordingly, to reduce the focal length of the laser beam.

The long focal length (1 m) limits the dimensions of the PLI to  $50 \times 40 \times 30$  cm. With such dimensions, the vacuum volume, the sensitive element and other structural parts made of stainless steel have a rather large weight ( $\approx 60$  kg).

It was necessary to drastically reduce the size and weight of the PLI. To do this, we used a new position-sensitive photometric method for detecting the displacement of a spot of a single-mode laser beam—the Dividing Plate method.

The position of the laser beam in the Dividing Plate method is determined using a specially prepared dividing plate. It is an optical plate with a sputtered metal (Ag) layer. The line of contact between the surface of the optical plate and the metal (division line) is a straight line (Fig. 12).

When focusing the laser beam on the division line of the dividing plate, one part of the laser beam is reflected from the metal film, and the other part passes through the transparent part of the optical plate. Further, they are sent to photodetectors PhD1 and PhD2. (Fig. 13).

The transverse displacement of the laser beam, which is proportional to the angle of inclination of the Earth's surface, leads to a change in the signals from the PhD1 and PhD2 photodetectors. As can be seen, this method is free from the dialectical gap that exists in a quadrant photodetector and, accordingly, it is possible to reduce the diameter of a focused laser beam to several microns.

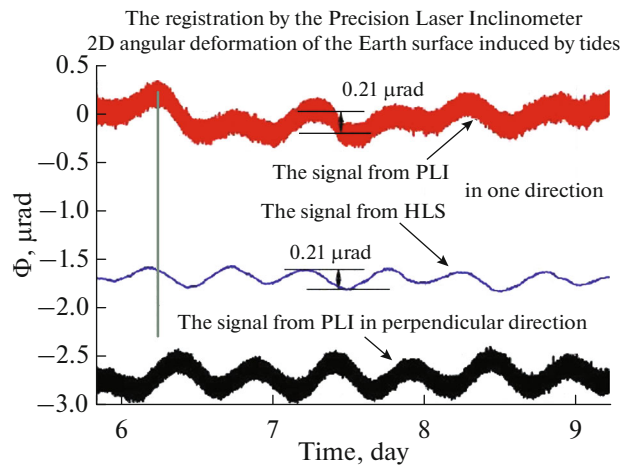


Fig. 8. Long-term registration of the inclinations of the earth's surface due to the Moon and the Sun.



Fig. 9. PLI of the fourth generation.

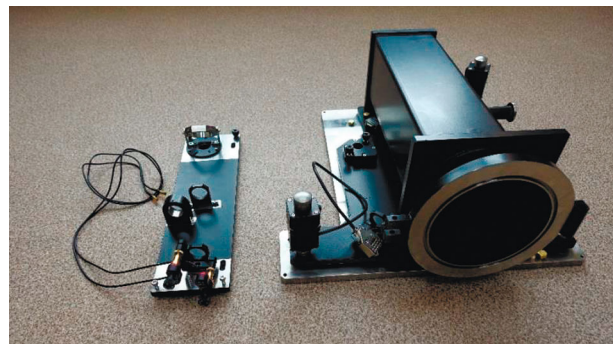


Fig. 10. PLI of the fifth generation.

Experiments with dividing plates made by us showed that signals of photodetectors did not have peculiarities in the zone of linear displacements. With a collated laser beam diameter of 6.8 mm, we managed to focus the laser beam to a spot with the diameter of

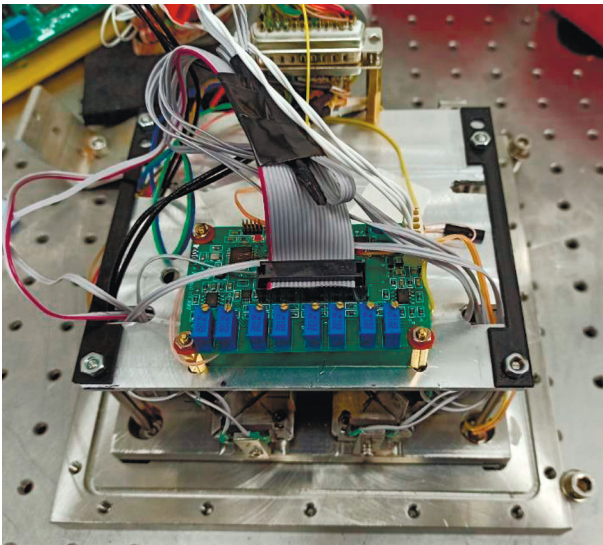


Fig. 11. Compact Precision Laser Inclinometer.

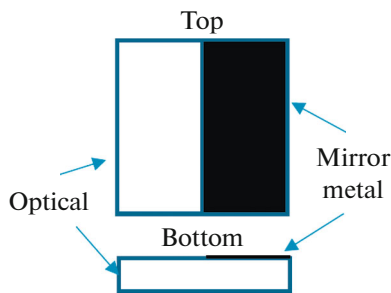


Fig. 12. Dividing plate.

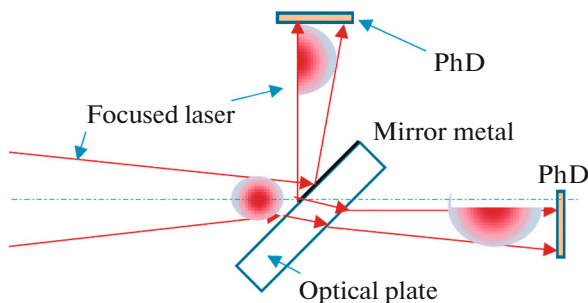


Fig. 13. Division of a focused laser beam with a dividing plate.

10  $\mu\text{m}$  at a focal length of 7.5 cm. Thus, we managed to reduce the focus length of the laser beam by more than a factor of 13 and thereby implement a compact PLI version.

#### *CPLI Scheme*

We managed to assemble all the optical elements of the inclinometer into a structure with dimensions of  $20 \times 20 \times 20$  cm.

Figure 14 shows the optical scheme of the inclinometer.

The CPLI used an S4FC637 laser (Thorlabs) with a fiber-optic output (radiation wavelength  $\lambda = 0.637 \mu\text{m}$ , radiation power 7 mW).

Laser radiation was fed through an optical fiber input into the vacuum volume of the CPLI. Then it was directed to optical cube no. 1 using a collimator. Half of the laser beam was used to form reference beams, and the other half was used to produce a signal beam. After reflection from the liquid surface, the laser beam was sent back to OK1, where half of its power entered the signal beam shaping unit. The reference and signal laser beams were formed using OC2 and OC3 and mirrors M1 and M2. They were fed to the position-sensitive photodetectors—Dividing Plates DP1, DP2, DP3, DP4—to analyze their displacement in two orthogonal directions (horizontal and vertical directions relative to the gravity vector were chosen). Two photodetectors were used in each Position Sensitive Device (PSD) Dividing Plate. Thus, in the system for recording angular positions of the signal and reference laser beams, there were eight information channels (1–8). Signals from the photodetectors were recorded by two four-channel Data Translation DT9824 ADCs and recorded into a computer.

Working on the CPLI, we abandoned the alignment of laser beams, as was the case in previous PLI generations. The main reason was that the alignment devices were a source of low-frequency noise. In the CPLI, all optical elements—a laser collimator, optical dividing cubes, lens mirrors—were mounted in block on a Special Platform (SP). The SP is fixed in one piece to the stationary CPLI platform, in which a cuvette with liquid is placed.

A feature of the CPLI is the transfer of all adjustment operations in the inclinometer to the adjustment of the PSD Dividing Plate. Adjustment of the PSD Dividing Plate with respect to the focus spot of the laser beam was carried out using piezoelectric linear positioners (NEWPORT AG-LS25). The dividing line of the dividing plate was set to the center of the focused laser beam using a piezoelectric positioner with an accuracy of the positioner minimum step of 100 nm. With a laser beam spot diameter of 18  $\mu\text{m}$ , such a step made it possible to accurately find the center of the laser beam and achieve equal power on the PSD Dividing Plate photodetectors PhD1 and PhD2.

All optical elements were attached to metal structural elements with glue.

The metal structure of the CPLI is made of stainless steel. This is because the CPLI is mounted on a concrete base. The linear expansion coefficient of steel is approximately equal to the linear expansion coefficient of concrete, which makes it possible to avoid deformation of the CPLI structure when the temperature changes.

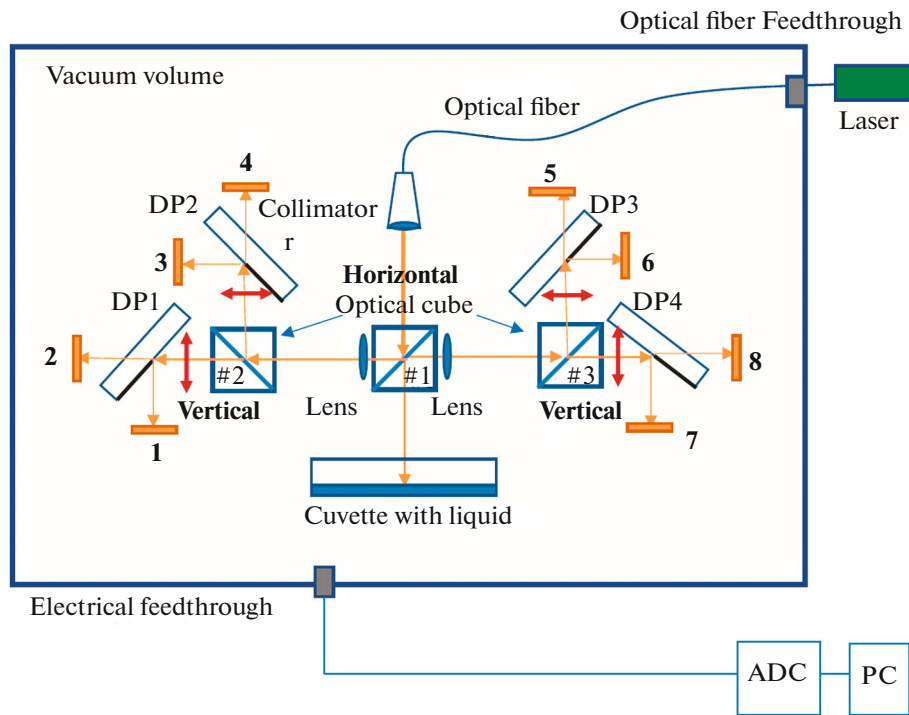


Fig. 14. Scheme of the CPLI.

To ensure solidity of the design, the calibration unit in the CPLI was made as an external independent device. Before using the inclinometer, the CPLI was calibrated. The aligned and evacuated CPLI was installed on a calibration device, on which the calibration coefficients were determined using the interferometric calibration technique.

The accuracy of the calibration device allows the calibration coefficients to be determined with an accuracy of 1%.

In 2021, the first CPLI prototype was assembled at the DLNP Metrological Laboratory.

After a number of modifications, we obtained the CPLI version that can be used both for the low-frequency region of the spectrum ( $<10^{-3}$  Hz) of angular seismic changes in the surface, and for the high-frequency region [ $10^{-3}$ –10 Hz], in which microseismic vibrations of terrestrial and industrial nature are concentrated.

*Signal Registration Scheme in CPLI*

The CPLI uses two types of signals.

— The first type of signals is associated with the chaotic angular motion of the laser beam, which is due to the temperature instability of the laser cavity and the optical fiber. These signals are recorded by DP1 with photodetectors FP1, FP2 and DP2 with photodetectors FP3, FP4.

— The second type of signals is associated with registration of the slopes of the earth’s surface by determining displacements of the laser beam reflected from the surface of the liquid. These signals are recorded using DP3 with photodetectors FP5, FP2 and DP6 with photodetectors FP7, FP8.

Thus, we have sets of signals from photodetectors (1–8):

- signals U1, U2 for the vertical direction of movement of the spot of the reference laser beam;
- signals U3, U4 for the horizontal direction of movement of the spot of the reference laser beam;
- signals U5, U6 for the horizontal direction of movement of the spot of the signal laser beam;
- signals U7, U8 for the vertical direction of movement of the spot of the signal laser beam.

The main idea of the technique for detecting the angular noise motion of a laser beam is its subsequent subtraction from the displacements of the laser beam reflected from the liquid. This procedure allows cleaning the signals from the noise of the angular movement of the laser beam.

Thus, the signal processing is determined by the formulas below.

First, we find the differences in the signals from the photodetectors for the reference and signal beams. This procedure reduces the effect of laser beam power instability and doubles the useful signal.

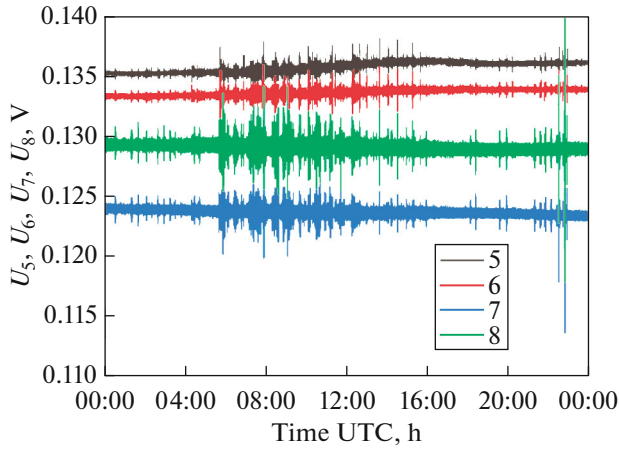


**Fig. 15.** One-day recording of four signals from signal photodetectors.

For reference beam

$$\Delta U_{12} = \frac{(U_1 - U_2)}{(U_1 + U_3)}; \quad \Delta U_{34} = \frac{(U_3 - U_4)}{(U_3 + U_4)}. \quad (3)$$

For signal beam

$$\Delta U_{56} = \frac{(U_5 - U_6)}{(U_5 + U_6)}; \quad \Delta U_{78} = \frac{(U_7 - U_8)}{(U_7 + U_8)}. \quad (4)$$

To reduce the influence of noise wandering of the laser beam, we successively subtract the signals of the reference beam  $\Delta U_{12}$  and  $\Delta U_{34}$  from the signals of the signal beam  $\Delta U_{56}$  and  $\Delta U_{78}$

$$U_{s1} = \Delta U_{78} - \Delta U_{12}, \quad U_{s2} = \Delta U_{56} - \Delta U_{34}. \quad (5)$$

Knowing the calibration coefficients  $K_{s1}$  and  $K_{s2}$ , we finally determine the angles of inclination of the Earth's surface in two orthogonal directions

$$\Phi_{s1} = K_{s1}U_{s1}; \quad \Phi_{s2} = K_{s2}U_{s2}. \quad (6)$$

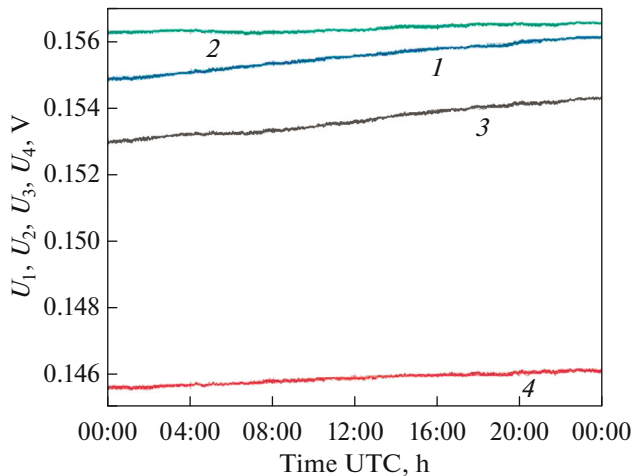


**Fig. 16.** One-day recording of four signals from reference photodetectors.

## EXPERIMENTS WITH CPLI

During the experiments, the CPLI was fixed to the concrete floor of the Metrological Laboratory. After several days of stabilization of the inclinometer position, eight CPLI signals were recorded within 24 h. The experiments were carried out in the absence of personnel, since the presence of people directly in the laboratory deforms the floor of the laboratory and causes spurious signals. The duration of one measurement was 1/30 s.

### Processing of Experimental Signals in the CPLI

Figures 15 and 16 show the form of the CPLI signals.

As can be seen from Fig. 16, registration of primary signals showed their sufficient stability and absence of significant long-term drifts.

According to the formulas (3), (4), difference signals  $\Delta U_{12}$ ,  $\Delta U_{34}$ ,  $\Delta U_{56}$  and  $\Delta U_{78}$  are defined.

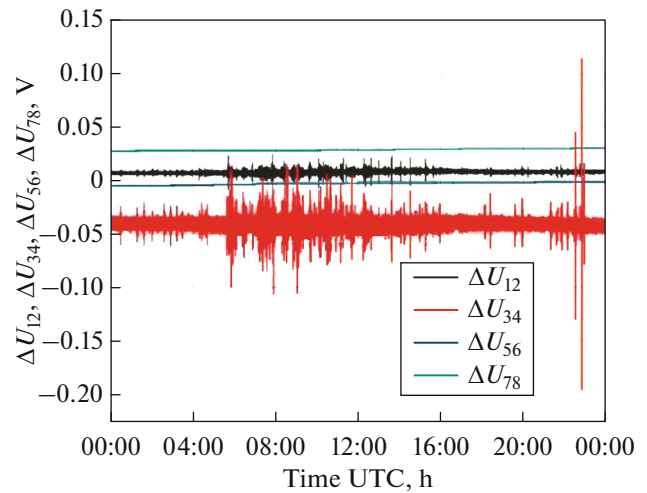
Figure 17 shows these signals.

As is evident from Fig. 17, the four processed signals are less dependent on the change in the power of the laser source.

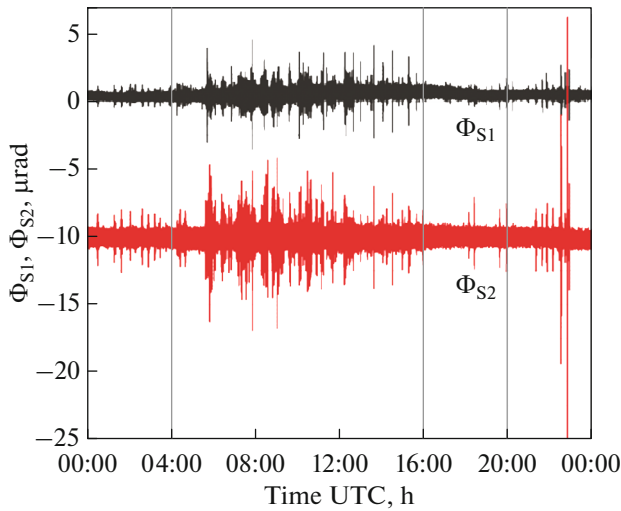
Then we subtracted the reference signals from the tilt signals and multiplied the result by the calibration coefficients  $K_{s1}$  and  $K_{s2}$  and finally determined two signals  $\Phi_{s1}$  and  $\Phi_{s2}$ , which correspond to the oscillations of the Earth's surface in two orthogonal planes.

Figure 18 shows the calculated signals  $\Phi_{s1}$  and  $\Phi_{s2}$  which take into account the effects of laser power instability and the angular noise motion of the laser beam.

The slopes of the Earth's surface  $\Phi_{s1}$  and  $\Phi_{s2}$  were measured in the East–West and North–South directions.



**Fig. 17.** Difference signals  $\Delta U_{12}$ ,  $\Delta U_{34}$ ,  $\Delta U_{56}$  and  $\Delta U_{78}$ .



**Fig. 18.** Processed signals of angular inclinations  $\Phi_{s1}$  and  $\Phi_{s2}$  of the Earth’s surface for a period of 24 h.

**CPLI CALIBRATION**

Calibration was carried out with an external calibration device.

In [7], we developed a procedure for calibrating an inclinometer using an interferometer. The essence of the calibration is to simultaneously change linearly increasing tilt angles with the help of an interferometer and an inclinometer while changing them linearly with the help of a piezo stacker. Figure 19 shows a diagram of an interferometric calibration block.

The CPLI and the interferometer are installed on the mobile platform of the calibration device. The movable platform can change the angular position relative to the fixed platform by a calibration angle using a piezo stacker. When a growing voltage is applied to the piezo stacker, the movable platform tilts relative to the ball, which leads to a change in the distance between the interferometer mirrors, a shift of the fringes in the interference pattern, and, accordingly, a change in the signal on the photodiode. Signals from the interferometer and the CPLI are fed to the ADC. With a continuous tilt of the moving platform, the signals from the CPLI and from the interferometer are simultaneously measured.

On Fig. 20 the data of recording signals from the CPLI and from the Interferometer are shown.

As is seen, the change in the Interference Pattern leads to a sinusoidal change in the calibration signal. Changes in the angles of inclination measured with the PLI have a linear form. Knowing that the distance between the IR maxima corresponds to  $\lambda/2$ , we can determine the calibration angle.

$$\Phi_k = \frac{N\lambda}{2L}, \tag{7}$$

where  $L$  is the distance between the interference block and the piezo stacker (Fig. 19), and  $N$  is the number of the maxima of the interference pattern.

Since the change in the angle  $\Phi_k$  and the signals  $\Delta U_{k1}$  and  $\Delta U_{k2}$  occur simultaneously, we can determine which change in the signal from the CPLI

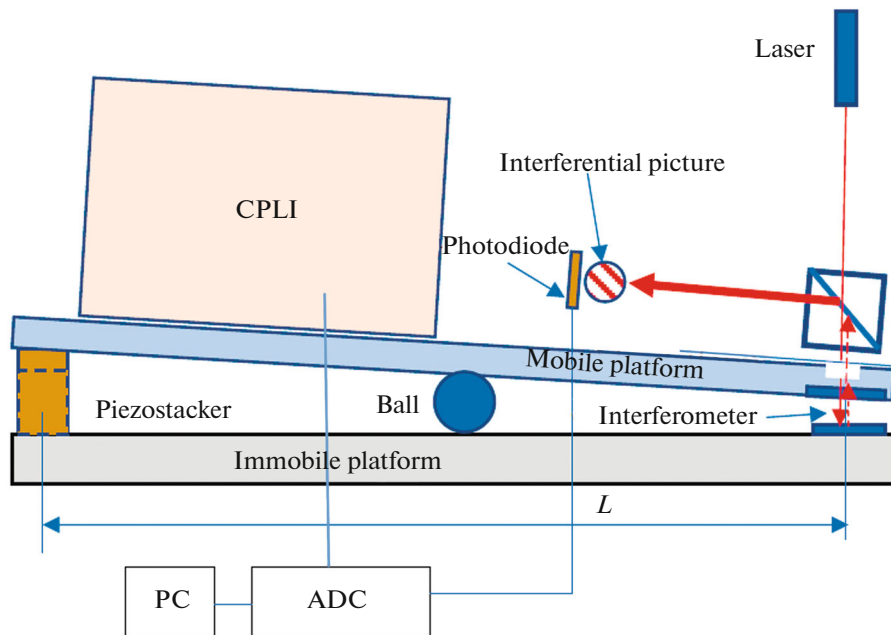


**Fig. 19.** Scheme of interference calibration of CPLI.



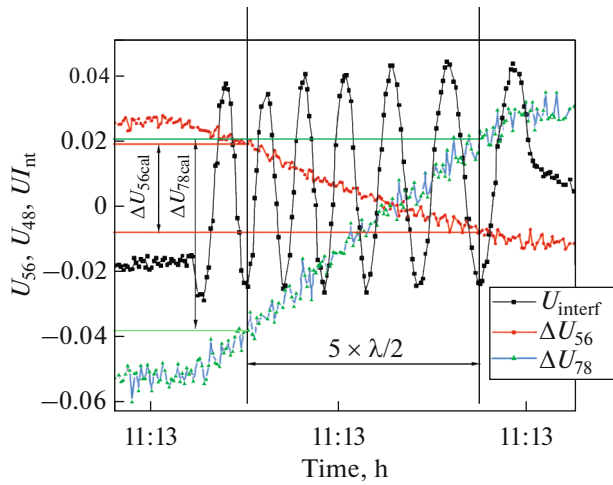


**Fig. 20.** Determination of calibration coefficients from measurement data.

$\Delta U_{k1}$  and  $\Delta U_{k1}$  corresponds to the change in the tilt angle by the calibration angle  $\Phi_k$ .

From formula (8) we determine the calibration coefficients.

$$K_{s1} = \frac{\Phi_k}{\Delta U_{k1}} ; K_{s2} = \frac{\Phi_k}{\Delta U_{k1}}. \quad (8)$$

The calibration coefficients  $K_{s1}, K_{s1}$  were determined based on ten independent calibration measurements. In each measurement, its own calibration coefficients were recorded, and then the average value of the calibration coefficients and their root-mean-square deviations were calculated.

The values of the calibration coefficients during the measurements (Fig. 18) are as follows:

— for the direction in which the signal laser beam moves horizontally (North–South),

$$K_{s1} = 225 \pm 3 \text{ } \mu\text{rad.}$$

— for vertical displacements (West–East),

$$K_{s2} = 105 \pm 2 \text{ } \mu\text{rad.}$$

*Registration of Microseismic Signals of the CPLI*

From the measurement data shown in Fig. 18, it can be seen that the main component of the signals corresponds to industrial noise. Moreover, industrial noise increases significantly during the daytime. Figure 21 shows the spectrum of floor movement oscillations in the frequency range  $1.4 \times 10^{-3}$ –12 Hz during the measurement time of 24 h in the East–West direction.

Figure 22 shows the spectrum of the floor movement oscillations in the frequency range  $1.4 \times 10^{-3}$ –12 Hz during the measurement time of 24 h in the North–South direction.

As can be seen from Figs. 21 and 22, signals of the Microseismic Peak in the frequency range of  $1.4 \times 10^{-3}$ –12 Hz, industrial noise associated with vehicle and rail traffic, and a signal from the rotation of hydro turbines at the Ivankovskaya HPP are observed.

Figures 23–25 show the appearance of the Microseismic Peak, rail traffic and remote earthquake signals.

*Measurement Accuracy and Noise of the CPLI*

The CPLI measurement accuracy is determined by the value of the minimum recorded microseismic signal. As a rule, the amount of noise is determined by the minimum value of the spectral density of microseismic signals recorded during a certain period of

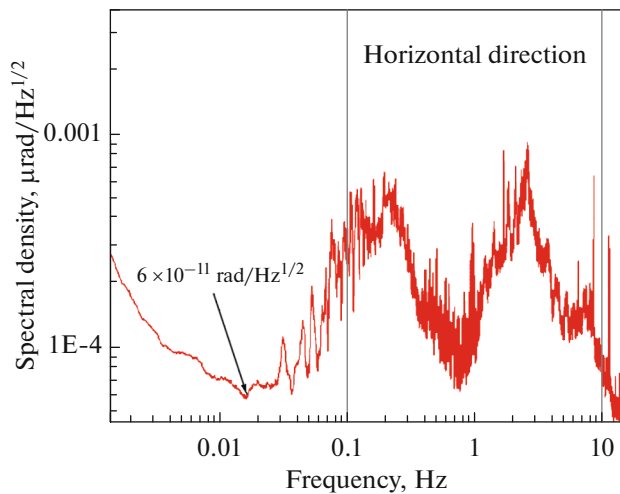


**Fig. 21.** Fourier analysis of the Earth’s surface oscillations in the East–West direction (data from Fig. 18).

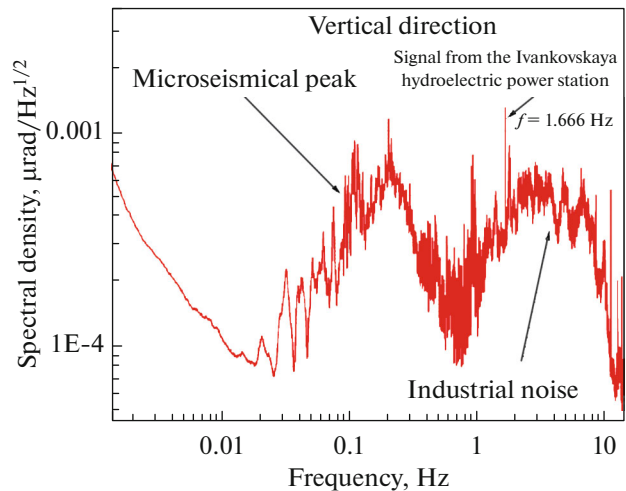


**Fig. 22.** Fourier analysis of the Earth’s surface oscillations in the North–South direction (data from Fig. 18).

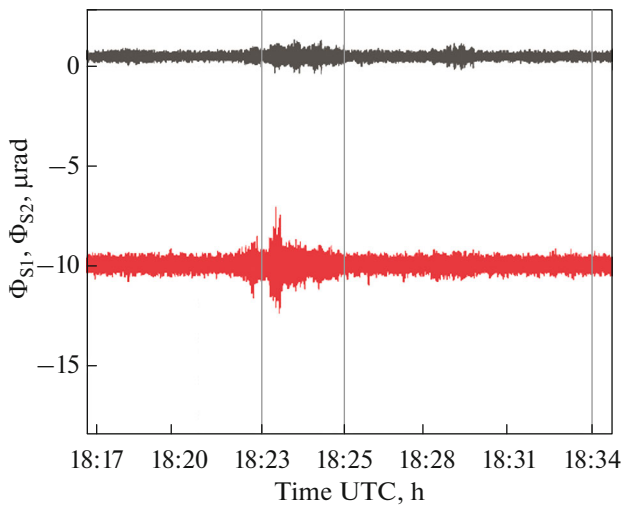


Fig. 23. Rail traffic signal.

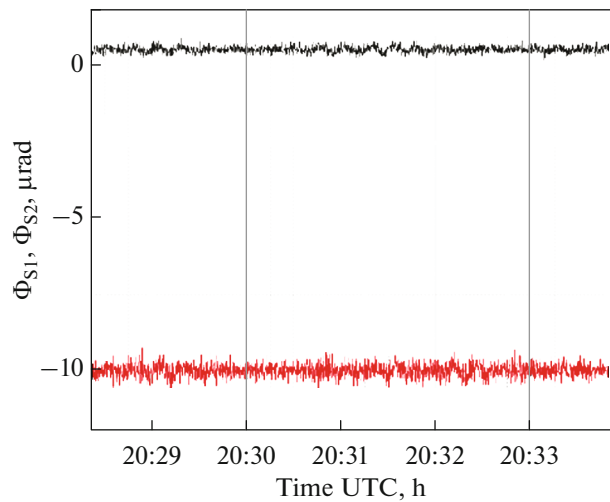


Fig. 25. Microseismic peak signals.

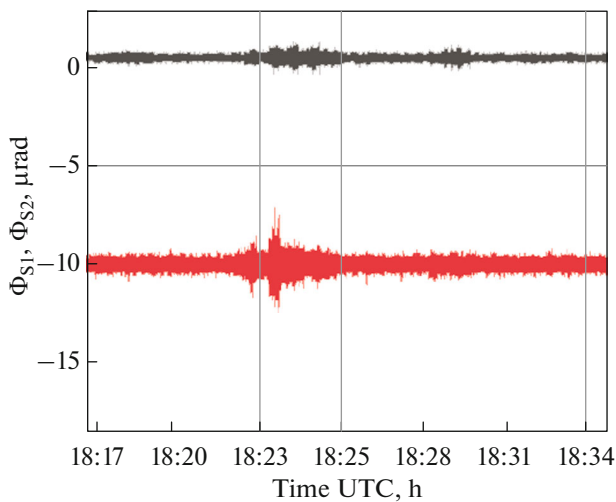


Fig. 24. Remote earthquake signal.

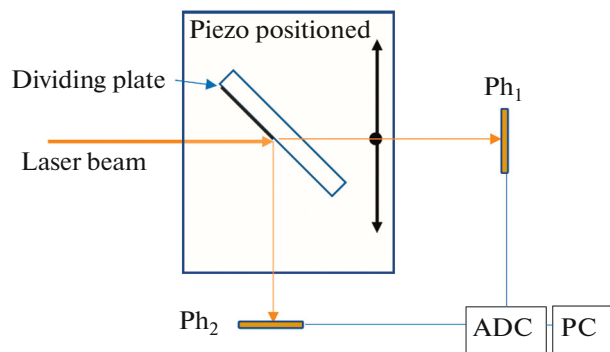


Fig. 26. Scheme of the experiment to determine the instrumental accuracy of the CPLI.

time. In our case, we traditionally use a day (24 h) as this period of time.

The value of the minimum spectral density is determined in the frequency range into which the majority of mycoseismic signals fall ( $10^{-3}$ – $10$  Hz). The problem of noise is related to the fact that in the spectrum of microseismic signals there are both narrow-band signals from the microseismic peak, earthquakes, industrial noise, etc., and broad-band ones from the movement of continents, magma, deformation of the earth’s surface under the influence of wind load and temperature, etc. Therefore, in seismometry, this level is set as the base level, and the sensitivity of the seismic instrument is determined by instrumental noise [26, 27].

The minimum value of angular oscillations was registered by us with the help of the PLI in Garni (Armenia). It was  $1.8 \times 10^{-11}$  rad/Hz<sup>1/2</sup>.

From the analysis of the data presented in Fig. 20, the value of the minimum signal that was registered in our case was  $6 \times 10^{-11}$  rad/Hz<sup>1/2</sup> (Fig. 20).

To determine the magnitude of instrumental noise, we used the movement of the dividing plate to the minimum possible distance. Figure 26 shows the scheme of the experiment.

The laser beam was sent to the dividing line of the dividing plate. The displacement of the laser beam on the dividing line was simulated by the transverse displacement of the dividing plate using a piezoelectric positioner. Signals from photodetectors were recorded by PhD1 and PhD2, ADC and processed by a computer.

The minimum possible displacement of laser beam was  $0.342 \pm 0.002$  μm. It was measured by moving the piezo positioner based on 10000 steps. The displacement of the piezo positioner carriage was determined

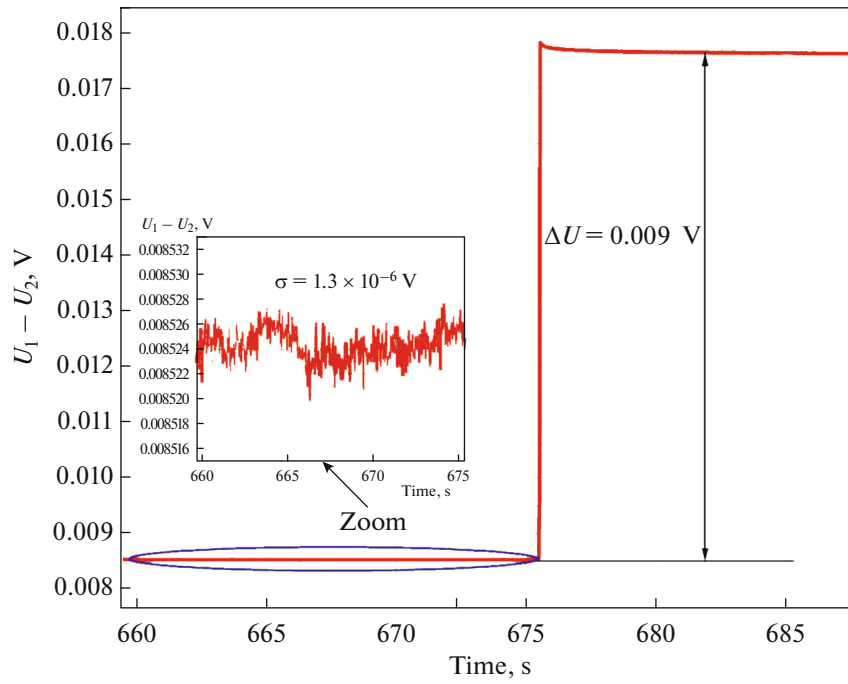


Fig. 27. Determining the magnitude of instrumental noise in the CPLI.

using a digital caliper. On the basis of multiple measurements, the average value of the minimum displacement and its accuracy were calculated.

Figure 27 shows the results of the laser beam spot displacement on the dividing plate when the laser beam spot is shifted by  $0.342 \mu\text{m}$ .

After determining the root-mean-square value of the noise of the reference beam  $\sigma(V)$  during the observation time of 15 s and measuring the change in the difference of signals  $\Delta U$  from photodetectors, we can calculate the displacement in dimensional values.

From the relation

$$\frac{\Delta U}{\sigma(V)} = \frac{0.342 \mu\text{m}}{\sigma(\text{m})}; \quad \sigma(\text{m}) = \frac{0.342 \mu\text{m}}{\Delta U} \sigma(V) \quad (9)$$

we determine the noise value  $\sigma(\mu\text{m})$  of the laser beam spot in meters. The value of the root-mean-square measurement accuracy was  $\sigma = 40 \text{ pm}$ .

With the known distance  $L$  from the optical fiber to the dividing line of the dividing plate ( $L = 10 \text{ cm}$ ) (see Fig. 14) inserted in the formula  $\sigma(\text{rad}) = (\sigma(\mu\text{m}))/L$ , the instrumental error  $\sigma_{\text{CPLI}}$  online measurement of CPLI was found to be  $\sigma(\text{rad}) = 5 \times 10^{-10} \text{ rad}$ .

Using formula (1), we also determine the calibration factor for the reference beam.

$$K_{\text{ref}} = \frac{\Phi}{\Delta U} = \frac{0.342 \mu\text{m}}{L \Delta U}. \quad (10)$$

For  $L = 10 \text{ cm}$ ,  $\Delta U = 0.009 \text{ V}$ .

$K_{\text{ref}} = 50 \mu\text{rad/V}$ .

By converting the data on the change in the reference beam from V to  $\mu\text{rad}$  using the calibration coefficient  $K_{\text{ref}}$ , we obtain the one-day instability of the reference beam in radians (Fig. 28).

Based on the data in Fig. 16, we determine the spectral density of the reference beam oscillations.

Figure 29 shows the Fourier analysis of the changes in the angular direction of the reference laser beam in the frequency range  $1.4 \times 10^{-3} - 12 \text{ Hz}$  obtained from the data of Fig. 28.

As can be seen from Fig. 29, the spectral density in the frequency range  $1.4 \times 10^{-3} - 12 \text{ Hz}$  varies from  $2.0 \times 10^{-10} \text{ rad/Hz}^{1/2}$  to  $1.6 \times 10^{-12} \text{ rad/Hz}^{1/2}$ .

## RESULTS AND DISCUSSION

The achieved dimensions and sensitivity of the CPLI are quite adequate for its use in the VIRGO second-generation IGA, in the LHC Tunnel, and also for earthquake prediction.

The IGA of the third generation requires a CPLI capable of operating at cryogenic temperatures. The main problem at such low temperatures is the supply of the cryogenic liquid to the working area of the CPLI. For this purpose, it is proposed to use a closed volume in which a liquefied gas is at atmospheric pressure (Fig. 30).

Upon reaching cryogenic temperatures, the gas liquefies, condenses and collects in a cuvette. In this case, the laser beam begins to be reflected from the surface of the cryogenic liquid and is used in the con-

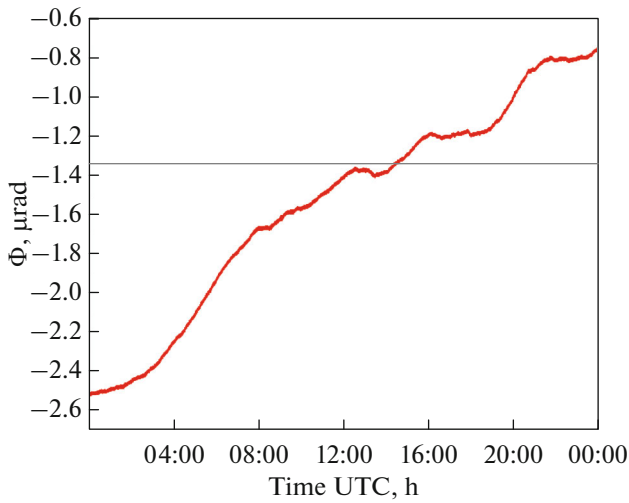


**Fig. 28.** Angular instability of the angular position of the reference laser beam.

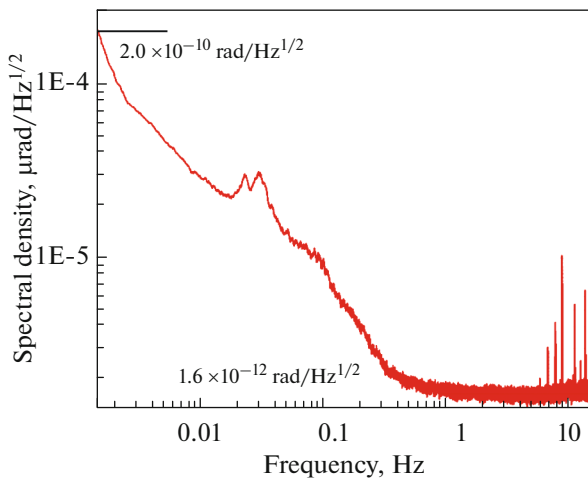


**Fig. 29.** Spectral density of the CPLI instrumental noise in the frequency range  $1.4 \times 10^{-3}$ –12 Hz.

ventional PLI scheme. Adjustment of the laser beam on the Position-Sensitive Photodetector Device is carried out using external piezo-stackers. They tilt the closed cuvette and thus adjust the laser beam reflected from the surface of the cryogenic liquid to the PSD. Since it is not necessary to stabilize the direction of the initial laser beam in the frequency range  $10^{-3}$ –20 Hz (see Fig. 14), the CPLI design is greatly simplified without reference beams.

This arrangement of optical equipment makes it possible to create a CPLI operating under cryogenic conditions, which will allow stabilizing the position of mirrors and dividing plates of the third-generation IGA “Einstein Telescope”.

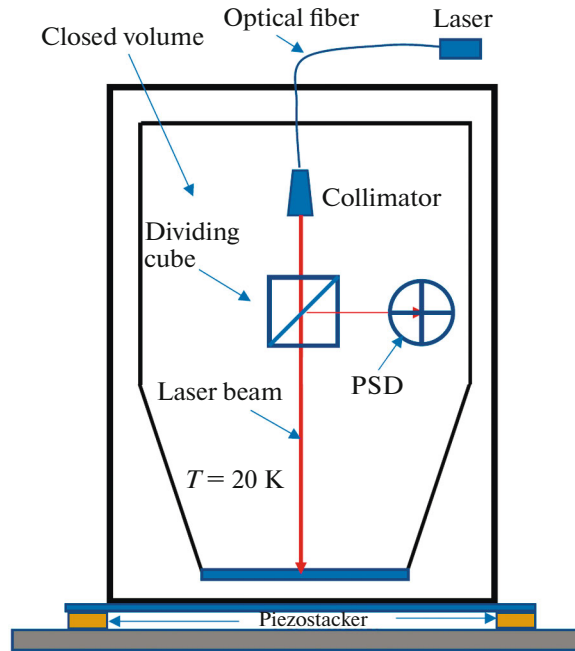


**Fig. 30.** Scheme of the cryogenic CPLI.

CONCLUSIONS

The results of the work of a new-generation PLI—the Compact Precision Laser Inclinator—are presented.

The overall dimensions of  $20 \times 20 \times 20$  cm and the weight of  $\approx 10$  kg have been achieved in the CPLI, which allows the CPLI to be used for stabilizing sensitive elements of the VIRGO second-generation interference Gravity Antenna and creating a network of inclinometers designed to stabilize the spatial position of the LHC collider and its long-term deformations. The new type of PLI will also enable creation of an earthquake forecasting network.

The CPLI measurements were carried out at the DLNP Metrological Laboratory (JINR). A 24 h record of the angular oscillations of the Earth’s surface in two orthogonal planes was obtained.

Sensitivity about  $6 \times 10^{-11}$  rad/Hz<sup>1/2</sup> was achieved in the frequency range  $10^{-3}$  to 12 Hz.

Microseismic oscillations of the Microseismic peak type, signals of remote earthquakes, and industrial noise were registered.

The instrumental angular accuracy of CPLI measurements is determined. For online measurements, it is 0.5 nrad. The spectral density of oscillations in the frequency range  $1.3 \times 10^{-3}$ –12 Hz varies from  $2.0 \times 10^{-10}$  rad/Hz<sup>1/2</sup> to  $1.4 \times 10^{-12}$  rad/Hz<sup>1/2</sup>.

A cryogenic version of the CPLI is proposed for the third-generation gravitational antenna “Einstein Telescope”.

## CONFLICT OF INTEREST

The authors declare that they have no conflicts of interest.

## REFERENCES

1. T. Westphal, H. Hepach, J. Pfaff, and M. Aspelmeyer, “Measurement of gravitational coupling between millimetre-sized masses,” *Nature* **591**, 225–228 (2021).
2. N. S. Azaryan, J. A. Budagov, M. V. Lyablin, A. A. Pluzhnikov, G. Trubnikov, G. Shirkov, O. Bruning, B. Di Girolamo, J.-Ch. Gayde, D. Mergelkuhl, and L. Rossi, “Colliding beams focus displacement caused by seismic events,” *Phys. Part. Nucl. Lett.* **16**, 377–396 (2019).
3. L. Trozzo and F. Badaracco, “Seismic and Newtonian noise in the GW detectors,” *Galaxies* **10**, 20 (2022).
4. F. Matichard, B. Lantz, R. Mittleman, K. Mason, J. Kissel, B. Abbott, S. Biscans, J. McIver, R. Abbott, S. Abbott, et al., “Seismic isolation of advanced LIGO: Review of strategy, instrumentation and performance,” *Classical Quantum Gravity* **32**, 185003 (2015).
5. J. Budagov and M. Lyablin, “Device for measuring the angle of inclination,” RF Patent No. 2510488, (30 May 2012).
6. B. Di Girolamo, J.-Ch. Gayde, D. Mergelkuhl, M. Schaumann, J. Wenninger, N. Azaryan, J. Budagov, V. Glagolev, M. Lyablin, G. Shirkov, and G. Trubnikov, “The monitoring of the effects of Earth surface inclination with the precision laser inclinometer for high luminosity colliders,” in *Proceedings of Russian Particle Accelerator Conference RuPAC2016, St. Petersburg, Russia, 2016*, pp. 210–212.
7. N. Azaryan, J. Budagov, J.-Ch. Gayde, B. Di Girolamo, V. Glagolev, M. Lyablin, D. Mergelkuhl, and G. Shirkov, “The innovative method of high accuracy interferometric calibration of the precision laser inclinometer,” *Phys. Part. Nucl. Lett.* **14**, 112–122 (2017).
8. N. Azaryan, J. Budagov, M. Lyablin, A. Pluzhnikov, B. Di Girolamo, J.-Ch. Gayde, and D. Mergelkuhl, “The compensation of the noise due to angular oscillations of the laser beam in the precision laser inclinometer,” *Phys. Part. Nucl. Lett.* **14**, 930–938 (2017).
9. N. Azaryan, J. Budagov, V. Glagolev, M. Lyablin, A. Pluzhnikov, A. Seletsky, G. Trubnikova, B. Di Girolamo, J.-C. Gayde, and D. Mergelkuhl, “Professional precision laser inclinometer: The noises origin and signal processing,” *Phys. Part. Nucl. Lett.* **16**, 264–276 (2019).
10. N. Azaryan, J. Budagov, V. Glagolev, M. Lyablin, A. Pluzhnikov, A. Seletsky, G. Trubnikov, B. Di Girolamo, J.-C. Gayde, and D. Mergelkuhl, “The seismic angular noise of an industrial origin measured by the precision laser inclinometer in the LHC location area,” *Phys. Part. Nucl. Lett.* **16**, 343–353 (2019).
11. J. Budagov, B. Di Girolamo, and M. Lyablin, “The compact nanoradian precision laser inclinometer—an innovative instrument for the angular microseismic isolation of the interferometric gravitational antennas,” *Phys. Part. Nucl. Lett.* **17**, 916–930 (2020).
12. J. Budagov, B. Di Girolamo, and M. Lyablin, “The methods to improve the thermal tolerance of the compact precision laser inclinometer,” *Phys. Part. Nucl. Lett.* **17**, 931–937 (2020).
13. P. Melchior, *Earth Tides* (Pergamon Press, 1966; Mir, Moscow, 1968).
14. E. I. Butikov, “Oceanic tides: A physical explanation and modeling,” *Computer Tools in Education*, No. 5, 12–34 (2017).
15. B. Le Mkhauty, *An Introduction to Hydrodynamic and Water Waves* (Pacific Oceanographic Laboratory, Miami, 1969).
16. P. V. Kovtunenkov, “Propagation of perturbations in a thin layer of a fluid stratified by viscosity,” *Bull. Novosibirsk State Univ. Ser.: Math., Mech., Informatics* **12**, 38–50 (2015).
17. P. A. Tipler, *Physics* (Worth Publishers, New York, 1980), Ch. 14
18. R. De Luca and O. Faella, “Communicating vessels: A non-linear dynamical system,” *Rev. Bras. Ensino Fis.* **39**, e3309 (2017).
19. J. Budagov, B. Di Girolamo, and M. Lyablin, “The methods to improve the thermal tolerance of the compact precision laser inclinometer,” *Phys. Part. Nucl. Lett.* **17**, 931–937 (2020).
20. V. Batusov, J. Budagov, and M. Lyablin, “A laser sensor of a seismic slope of the earth surface,” *Phys. Part. Nucl. Lett.* **10**, 43–47 (2013).
21. V. Batusov, Y. Budagov, M. Lyablin, and A. Sissakyan, “On some new effect of laser ray propagation in atmospheric air,” *Phys. Part. Nucl. Lett.* **7**, 359–363 (2010).
22. V. Yu. Batusov, Yu. A. Budagov, M. V. Lyablin, and A. N. Sisakyan, “Device for forming a laser beam,” RF Patent No. 2510488 (30 May 2012).
23. M. Lyablin, “Observation of the 2-D Earth surface angular deformations by the Moon and Sun by the precision laser inclinometer,” in *Proceedings of the Challenge on Learned Image Compression (CLIC) Workshop* (2017).
24. W. Coosemans, H. Mainaud Durand, A. Marin, and J.-P. Quesnel, “The alignment of the LHC low beta triplets: Review of instrumentation and methods,” in *Proceedings of the 7th International Workshop on Accelerator Alignment, SPring-8, Japan, 2002*.
25. [www.hamamatsu.com/eu/en/product/optical-sensors/photodiodes/si-photodiode-array/segmented-type-si-photodiode/S5980.html](http://www.hamamatsu.com/eu/en/product/optical-sensors/photodiodes/si-photodiode-array/segmented-type-si-photodiode/S5980.html).
26. J. N. Brune and J. Oliver, “The seismic noise of the Earth’s surface,” *Bull. Seism. Soc. Am.* **49**, 349–353 (1959).
27. D. E. McNamara and R. P. Buland, “Ambient noise levels in the continental United States,” *Bull. Seism. Soc. Am.* **94**, 1517–1527 (2004).